lubricants

Article

Analysis of Tool Wear and Counter Surface Roughness in the Flexible Abrasive Tool Finishing

Mayank Kumar, Ajay Sidpara * and Vikranth Racherla

Department of Mechanical Engineering, Indian Institute of Technology, Kharagpur 721302, India
* Correspondence: ajaymsidpara@mech.iitkgp.ac.in

Abstract: This work uses the solvent casting method to fabricate an elastomeric tool with polyurethane as the base material and silicon carbide (SiC) as embedded abrasive particles. The distribution of abrasive particles and the pore structure in the fabricated tools are analyzed. The fabricated tools are porous in nature and have self-replenishing as well as self-lubrication properties. Aluminum 6061 alloy and electroless nickel-phosphorus plating having different initial roughness are selected as workpieces to study the wear mechanisms and loading of the flexible abrasive tool. The rotational speed of the tool, tool compression, and feed rate are fixed input process parameters. Total finishing time, sliding distance, and roughness are varied to obtain output responses. The workpiece material is also taken into account as a variable parameter in this study. These materials are classified as different counter surfaces as their surface roughness and mechanical properties vary. The finishing time and sliding distance for these counter surfaces differ in order to relate their effects on tool wear and loading. The nickel-plated surface shows a higher percentage reduction in surface roughness of 92% as compared to the aluminum surface, with a 62% reduction in surface roughness. The coefficient of friction, wear, and tool condition are analyzed to understand the mechanism of tool wear and tool loading. In this process, both two-body and three-body abrasions occur simultaneously and continuously.

Keywords: solvent casting; wear mechanisms; electron microscopy; characterization; adhesion; surface roughness

Citation: Kumar, M.; Sidpara, A.; Racherla, V. Analysis of Tool Wear and Counter Surface Roughness in the Flexible Abrasive Tool Finishing. *Lubricants* **2022**, *10*, 318. https://doi.org/10.3390/lubricants10110318

Received: 26 October 2022
Accepted: 16 November 2022
Published: 18 November 2022

1. Introduction

Elastomeric materials are used in many applications, such as the automobile industry, sealants, abrasive tools, and agricultural equipment. In many applications, the wear study of elastomers in different operating conditions is essential in product selection and prediction of product life. However, estimating elastomeric wear is challenging as the wear mechanism changes with different material properties and operating conditions. The wear of elastomers is generally affected by variables such as normal load, sliding distance, sliding velocity, rotational speed, temperature, running duration, surface properties of the counter surface, and abrasives [1,2]. Moreover, the material properties also play an important role in wear rate. Modeling of wear for elastomers is limited as compared to metals and their alloys. In general, experimental data obtained for elastomers is fitted into empirical equations for the wear modeling in most of the studies. Contradicting results are presented by Lancaster [3] and Rhee [4], where both linear and non-linear relations between wear volume and operating variables are established. Moreover, Viswanath and Bellow [5] considered the roughness of the counter surface as an additional parameter to develop a relation between wear rate and input variables. Panda et al. [6] proposed a model for the wear of polymers considering the topography of the counter surface. Different wear mechanisms exist when an elastomer rolls and slides against a relatively more rigid surface. These wear mechanisms are Schallamach waves, abrasion, fatigue, adhesion, and roll formation [1,7,8]. The descriptions of these wear mechanisms are listed in Table 1.

Table 1. Wear mechanisms of elastomer.

Types of Elastomeric Wear	Cause
Schallamach waves	"Waves of detachment" is the source of relative motion between the two frictional elements.
Abrasion	Scratched by a rough surface with protruding points.
Fatigue	Surface fatigue due to repeated loading.
Adhesion	Rubbing on a smooth surface. Asperities on the surface are distorted plastically, held together by the intense pressure, and fracture as the movement progresses.
Roll formation	Rolling of wear particles due to interfacial friction.

Polyurethane is one of the most used materials for polishing pads and tools used in the finishing process because of its superior mechanical, physical, thermal, and chemical stability. In optics and related fields, polyurethane pads with porous structures are widely used for various polishing purposes [9]. The elastic behavior of the polyurethane-based tools is affected by the working environment, i.e., temperature, loading frequency, and wetting conditions [10]. The elastic modulus and hardness of polyurethane are related to each other. The hardness of polyurethane tools can be influenced by several factors, including tool wear, the inclusion of debris, and loose abrasive particles, which further impact the quality of the finished surface. The finishing of gears, optical materials, bearings, and medical implants is carried out using elastic grinding wheels. The major disadvantage of using these elastic grinding wheels is that the material used for tool fabrication are thermoset, and it is chemically cross-linked, which limits the remolding of the wheels [11]. The commercially used flexible tools are fabricated by Tyrolit Group, Abtex LLC, and Misumi Corporation. These commercially available tools are mainly used as a substitute for rigid grinding tools and are commonly used for deburring, scratch removal, and fine grinding. The finishing of different components to a nanometer level using these commercially available tools is rarely addressed. The tool developed in this work can finish different components to a nanolevel finish at a good finishing rate.

Flexible abrasive tool finishing (FATF), also known as bonded abrasive tool finishing, is a technique used for finishing a wide variety of materials, particularly optical components. There are different issues associated with the finishing techniques used in the previous works. The most common problems are low finishing rates, environmental issues, excessive tool loading, and higher tooling costs. These problems can be overcome with the help of the fabricated tool in this work. This tool has a self-replenishing ability and is also flexible, which helps with uniform finishing. There is no environmental concern while using this tool. The fabrication technique is cost-effective. However, tool loading is a concern for the developed tool. Therefore, the performance of this tool is analyzed to correlate the loading and tool wear with the operating conditions. These tools have embedded abrasive particles that can conform to the shape of the workpiece surface. The porous open-cell structure allows for the retention of lubricants during the finishing experiments. The properties of flexible tools, such as their porosity, hardness, and elastic modulus, are related to their finishing ability. In the grinding and fine-finishing of components, tool wear and tool loading affect the tool performance and thus reduce the overall efficiency of the process. The quality of the finished surface depends on the wear and loading of the flexible abrasive tool. The wear of the flexible tools is related to their characteristics and the process parameters used in the finishing process. It is reported that polyethylene wear increases with the roughness of the counter surface [12]. The adhesive wear mechanism is observed when sliding polyketone and polytetrafluoroethylene against different counter surfaces [13]. An increase in the roughness of the counter surface leads to a lower coefficient of friction for polymer composites and elastomers [14,15].

In the present work, the effect of surface properties of different counter surfaces on the wear of the fabricated tools and the loading of these tools is studied. The effect of morphology and wear of polyurethane-based flexible abrasive tools having porous structures on the mechanism of material removal is also discussed. After finishing, the morphological study and weight loss analysis of the used flexible tools are carried out. It is observed that these tools are less resistant to wear, but as the process progresses, the wear of the tools reduces. However, various modifications to the tool microstructure and composition have been observed. The inclusion of chips in the microstructure of the tools, which alters their characteristics, is the most apparent change observed after the finishing operation. As the tool material is very soft and has pores, chips find difficulty escaping from the finishing zone as these chips are likely to get stuck in the tool material. During the finishing, some of the chips may be thrown away due to centrifugal force, but new chips get removed from the workpiece and stick to the tool. So, it is a reoccurring process. These chips are not participating in the material removal but abrade the surface depending on the rotational speed of the tool. The loose particles are abrasives that have fallen out of the polymer matrix. These abrasive particles are not completely removed from the finishing zone as some of them escaped from the finishing zone, and a few more will be separated from the tool during the finishing action. The self-replenishing property of the tool helps introduce new abrasives to facilitate finishing operations.

2. Materials and Methods

2.1. Materials

Solvent casting is used to create the flexible abrasive tool. At room temperature, polyurethane (PU) pellets are dissolved in a solution of tetrahydrofuran (THF) and dimethylformamide (DMF). THF is a widely utilized solvent for chemical synthesis. DMF is a unique solvent having a broad solubility range. Moreover, DMF has a significant affinity for creating elastomers with polyurethane as a base material. The dissolution process is carried out on a hot plate. Based on the previous studies, the weight percentage of polyurethane is selected. These PU pellets are synthesized using thermoplastic polyurethane (TPU), which can be recycled and has a superior elastic property [16,17]. After the complete dissolution of PU pellets, the abrasive particles are added to the solvent mixture. Silicon carbide (SiC), with an average size of 4 microns and a Mohs hardness grade of 9, is used in tool fabrication as abrasive particles. Figure 1 shows the flexible tool fabrication process. The polymer solution is thoroughly mixed with the abrasive particles before being poured into the desired shape and allowed to dry in the ambient air. The dissolution process was carried out at room temperature for five hours, and the stirring speed was 1000 RPM. PU pellets and abrasive particles are added in weight percentage (wt.%) corresponding to the volume of the solution. The mixing was carried out on a magnetic stirrer. The sinking of particles was not observed during the mixing process. However, loose abrasive particles are observed when higher weight percentages of abrasive are used for tool fabrication. The tools are removed from the mold after six days, and any solvent is removed with deionized water.

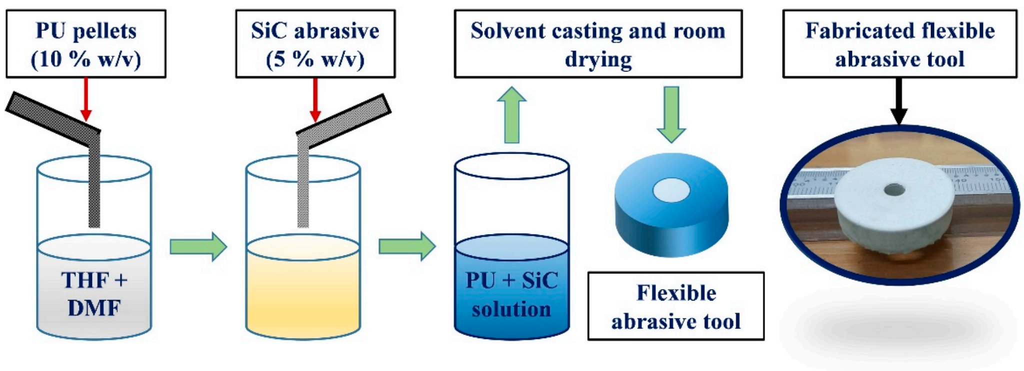

Figure 1. Flexible abrasive tool fabrication process and photograph of fabricated tool.

2.2. Mechanical Behavior and Characterization

The scanning electron microscope (EVO 18 Research, Zeiss, Oberkochen, Germany,) is used for studying the pore structure and abrasive particle dispersion of abrasive tools. Shore A durometer is used to measure the hardness of the tool. DMA 242E Artemis, NETZSCH is used to carry out the dynamic mechanical analysis to obtain the elastic properties of the fabricated tools. At a feed rate of 10 mm/min, the counter surface is translated against the rotating tool. The total running time for surfaces made of electroless-nickel phosphorus-plated stainless steel (NiP_SS316L) and aluminum alloy 6061 (Al 6061) is 2 min and 8 min, respectively. These materials are preferred for the mirror materials used in the telescope, defense, and space industries. The composition of Al 6061 is 97.9% Al, 1% Mg, 0.6% Si, 0.3% Cu, and 0.2% Cr. The density of Al 6061 is 2700 kg/m^3, and hardness is 107 HV. The NiP_SS316L is plated with a composition of 90% nickel and 10% phosphorus. It has a hardness of 620 HV. The substrate material SS316L is mainly composed of Fe, Cr, Ni, C, and Mo. Normal and tangential forces are measured using a load cell to determine the coefficient of friction. The weight loss method is used to measure tool wear. The loading of the tool is studied by the elemental mapping of the used tool. An optical 3D profilometer (CCI-MP, Taylor Hobson) is used to study the topography of the surface. The initial areal surface roughness (Sa) of Al 6061 and NiP_SS316L is 296 nm and 1034 nm, respectively.

2.3. Flexible Abrasive Tool Finishing

The tribological and finishing performances of the fabricated tools are investigated on a computer numerical control (CNC) machine having 4-axis control with a spindle oriented horizontally. The experimental setup for flexible abrasive tool finishing is shown in Figure 2. Spindle speed and tool compression are kept fixed at 2000 RPM and 2 mm, respectively. The diameter of the tool is 30 mm, and its thickness is 8 mm. The parameters are selected based on the trials and previously published work. The flexible abrasive tool has better performance when the rotational speed of the tool is varied between 1500 and 2000 RPM, and tool compression is 1.5 to 2 mm [18]. The fabricated tools are soaked in deionized water before the experiments, and no additional coolant is supplied during the finishing. The experiments are performed at room temperature to avoid any effect of temperature and humidity on the performance of the tool during the finishing process. The areal surface roughness of the counter surfaces varies to obtain the wear response of tools in terms of their areal surface roughness (Sa). The fixed parameters are the rotational speed of the tool, tool compression, and feed rate. The parameters that vary, apart from the initial roughness of the counter surface, are sliding distance and running time.

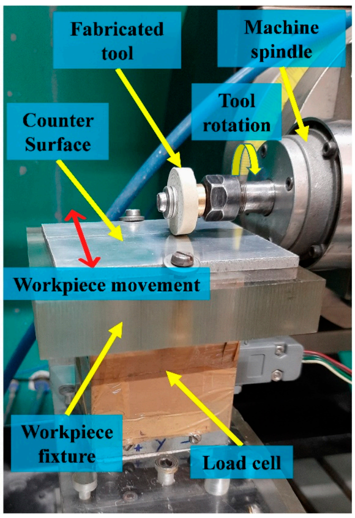

Figure 2. Flexible abrasive tool finishing experimental setup.

2.4. Wear Mechanism of Flexible Abrasive Tool

When the abrasive particles are embedded in the polymer matrix, they slide over the workpiece surface. Due to this interaction, the peak of the asperities is being sheared off due to abrasive action. It is related to two body abrasions [19]. The embedded abrasive particles have a significant effect on tool wear. If the size of the abrasive particles is larger than the spacing of the workpiece asperities, then the wear mechanism is related to the abrasion of abrasive particles. In contrast, if the size of the abrasive particles is on par with the spacing, it can lead to pull-out of the abrasive particles and, consequently, increase the tool wear [20]. Some abrasive particles are detached from the polymer matrix as the finishing process progresses due to tool wear. As a result, the detached abrasive particles act as loose abrasives during the process. Thus, the 2-body abrasion changes into the 3-body abrasion, with these loose abrasive particles also participating in material removal [21]. A schematic of abrasive particle interaction with the workpiece is shown in Figure 3.

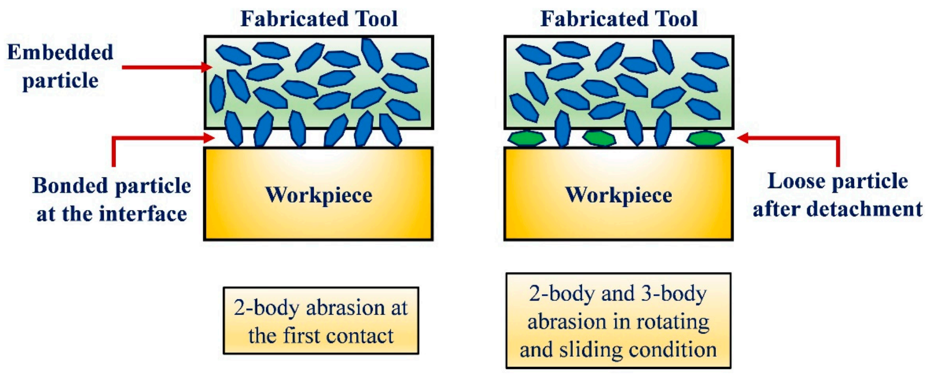

Figure 3. Schematic of abrasives interaction with the workpiece.

3. Results and Discussion

3.1. Microstructure of the Fabricated Tool

A small portion of the fabricated flexible abrasive tool is analyzed in SEM, as shown in Figure 4. The foamed structure bonds abrasive particles, and the pores in fabricated tools are open and interconnected. Open pores help in fluid absorption, retain lubricants and release them when pressed on the workpiece. This can be termed a self-lubricating property [18], and it is very useful in the finishing process. The abrasive embedment can be proven with the cross-section SEM image of the flexible tool. It can be seen that the abrasive particles are there in the cut part, which suggests that the abrasive particles are properly embedded in the foamed structure. As these tools can easily absorb the DI water, it can be concluded that the pores are open and interconnected. The solvent casting method allows for creating voids in the foamed structure, which results in interconnected pores. These open-cell foams can absorb and retain more fluid as compared to closed-cell foams.

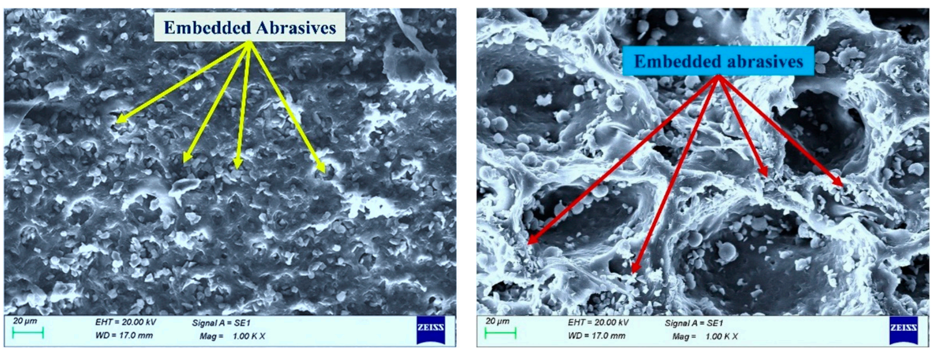

Figure 4. SEM image of fresh flexible abrasive tool: top surface (**left**) and cross-section (**right**).

Energy dispersive X-ray spectroscopy (EDS) is used for element mapping of the new flexible abrasive tool, as shown in Figure 5. The elemental mapping confirms the distribution and existence of abrasive particles within the foamed structure.

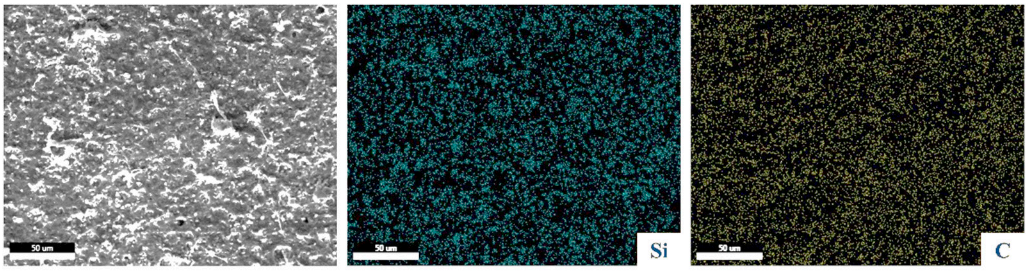

Figure 5. Elemental mapping of fresh flexible abrasive tool.

3.2. Elastic Property of the Fabricated Tool

Dynamic Mechanical Analysis (DMA) is carried out in compression mode to measure the elastic properties of the tools. The storage modulus, loss modulus, and damping factor are obtained. The damping factor is the ratio of the loss modulus to the storage modulus. Shore hardness testing is another method to measure the elastic property of the soft tool. Moreover, the shore hardness and abrasive wear of polyurethane are interrelated. The frictional heat generated at the interface is responsible for an increase in temperature, resulting in polyurethane softening. It is found that polymers having a Shore A hardness of less than 75 are affected by the temperature rise and become less wear-resistant [22]. The elastic modulus and shore hardness are related by Gent's equation, as given by Equation (1) [23]. The results from the DMA and shore hardness test, along with the estimated elastic modulus, are presented in Table 2. Measured and estimated values are close to each other.

$$E_t(N/\mathrm{mm}^2) = \frac{0.713428 * (56 + 7.66S)}{(254 - 2.54S)} \quad (1)$$

where E_t is the elastic modulus of the tool, and S is the Shore A hardness.

Table 2. Elastic properties of polymer tool measured using DMA and shore hardness test.

	Parameters	Values
DMA	Storage modulus	0.75 MPa
	Loss modulus	0.11 MPa
	Damping factor	0.14
Shore hardness test	Shore A hardness	20
	Elastic modulus (Gent's eq.)	0.73 MPa

3.3. Characterization of the Finished Surface

The line polishing experiments using the flexible abrasive tool on aluminum alloy 6061 and electroless nickel-phosphorus-plated stainless steel (NiP_SS316L) are carried out to analyze the finishing performance and wear of the tool. During the finishing process, the normal cutting force increases, followed by a fall and stabilization. During the initial phase, the tool is compressed to a specific value, increasing the normal cutting force. As soon as the tool rotation begins, certain abrasive particles and polymer material are sheared away due to rubbing with significant surface peaks. The tool then adjusts to ensure proper contact with the irregularities in the workpiece. At the same time, the tool is loaded with debris from the surface of the workpiece. The simultaneous occurrence of tool wear and loading is a complicated phenomenon. In an ideal scenario without tool wear, machining chips get attached to the tool surface as finishing advances, increasing the normal cutting force.

Figure 6 shows the normal cutting force vs. time graph for finishing Al 6061 and NiP_SS316L surfaces. It can be seen in the graph that there is a sharp decline in the normal cutting force for the Al 6061 surface. That can be attributed to the sticking tendency of the aluminum surface. The wear mechanism that can be related to this condition is adhesion. As the finishing process progresses, the pull-outs of the tool material decrease as the tool gets loaded with microchips that stick around the porous structure. The normal cutting force in the case of NiP_SS316L is higher when compared to Al 6061 can be attributed to the hardness of these materials. Despite the significant difference in the hardness of these two surfaces, the peak difference in normal cutting force is less than 1 N within the first 20 s. This can be related to tool flexibility, which helps the tool conform to the surface. As the finishing cycle progresses, the difference in normal cutting forces between the two surfaces increases due to the sticking tendency of the aluminum, which in turn results in tool material pull-outs.

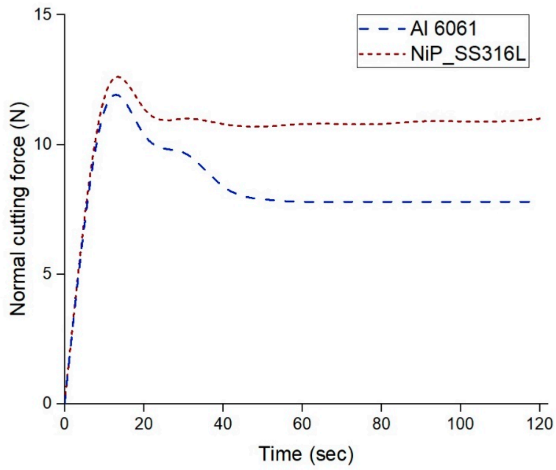

Figure 6. Normal cutting force vs. time for Al 6061 and NiP_SS316L surfaces.

The SEM image of the used tool for Al 6061 gives information about the different tool wear mechanisms, which are the primary reason for the sharp decline in normal cutting forces. Al 6061 is soft and sticky material, while nickel is comparatively hard and non-sticky. Therefore, material removal is easy in the case of nickel polishing as compared to Al 6061. Figure 7 shows the coefficient of friction (CoF) in line polishing Al 6061 and NiP_SS316L. The CoF decreases for the NiP_SS316L surface. This finding is in line with the literature where it is stated that the coefficient of friction decreases with the increase in roughness of the counter surface [13,14].

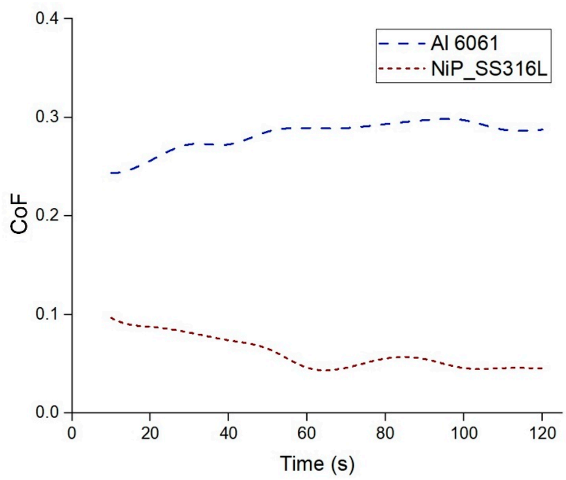

Figure 7. Coefficient of friction (CoF) in line polishing of Al 6061 and NiP_SS316L.

Figures 8 and 9 show the 3D surface profiles and 2D profile curves of the Al 6061 and NiP_SS316L surfaces before and after the line polishing experiment. The finishing is carried out in the direction perpendicular to the grinding marks on Al 6061. The percentage reduction in Sa is approximately 62% and 92% for aluminum and nickel-phosphorus-plated surfaces, respectively. The variation in the results can be related to the deeply indented abrasives being pulled out and adhered to the outer surface, resulting in an increment of the valley depth in the aluminum surface. However, the tool performs better on the nickel-phosphorus-plated surface as the higher surface peaks are removed relatively easily. Moreover, there is no sticking tendency on this surface like aluminum, which results in better interaction of the abrasives and consistent material removal from the nickel-phosphorus-plated surface. These findings will be evaluated with the bearing area curve, the characterization of the tool, and the finished surfaces.

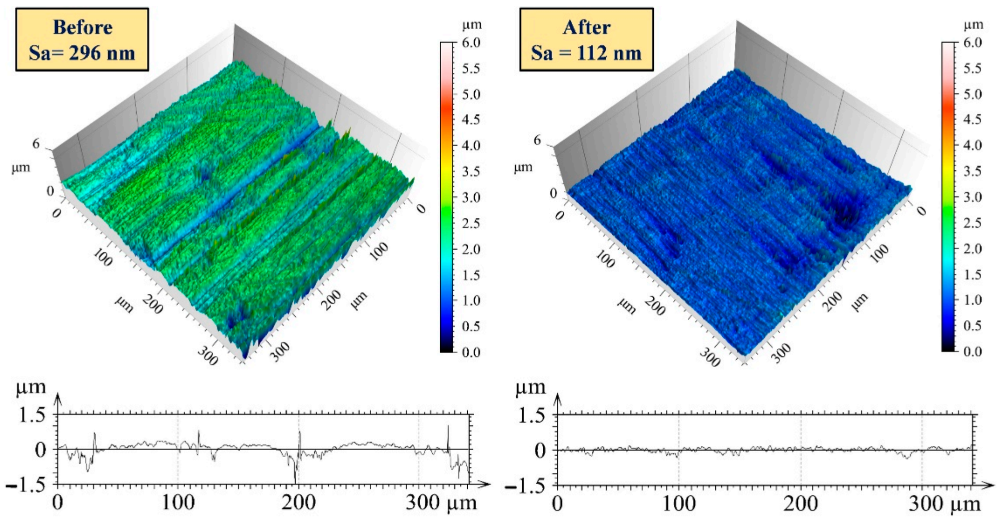

Figure 8. 3D surface profile and 2D profile curve of Al 6061 surface.

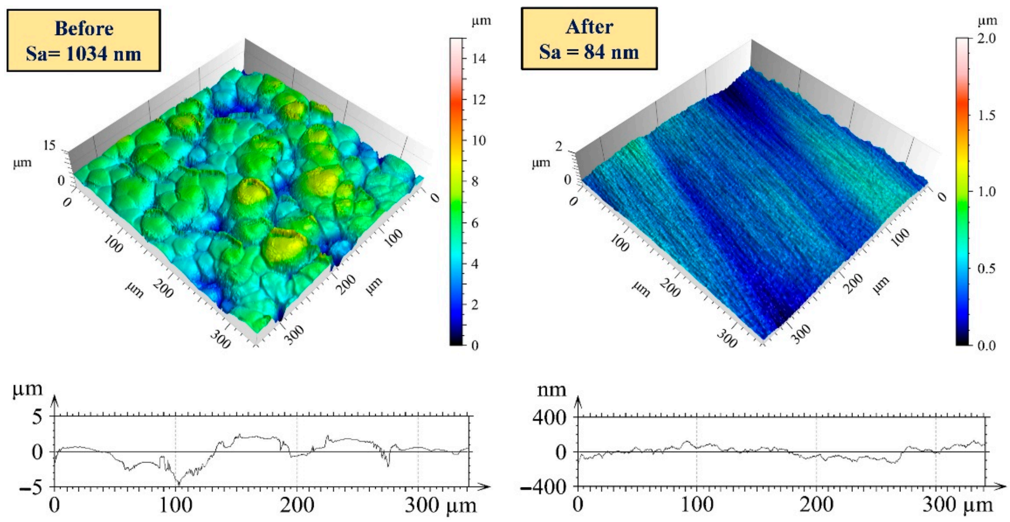

Figure 9. 3D surface profile and 2D profile curve of NiP_SS316L surface.

The bearing area curve (BAC), also known as the Abbott–Firestone curve or areal material ratio curve, is related to functional parameters used for analyzing the topography of the surface [24]. The schematic of BAC is shown in Figure 10, and the description of functional parameters is listed in Table 3.

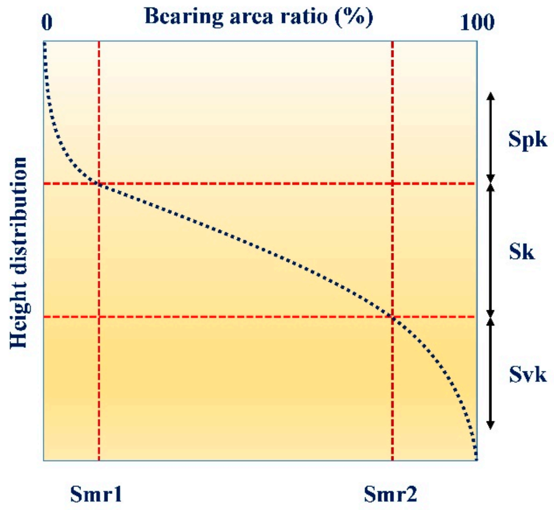

Figure 10. Schematic of bearing area curve (BAC).

Table 3. Parameters associated with bearing area curve (BAC) [24].

Parameters	Description
Sk (Core height)	The core surface height which is responsible for the service life of the component.
Spk (Reduced peak height)	Peak height above core surface height is responsible for effective contact area during mating.
Svk (Reduced valley height)	Valley depth below core surface height helps in lubrication retention.
Smr1 (Peak material portion)	The areal material ratio separates reduced peaks from the core surface.
Smr2 (Valley material portion)	The areal material ratio separates reduced valleys from the core surface.

This curve gives information on functional behaviors like lubrication retention capacity, surface peaks and asperities, and the effective contact area between mating parts depending on the wear of the surface. Kumar et al. [25] used BAC to estimate the component wear by implementing the numerical procedure for depth calculation. The wear will change the topography of the surface as well as introduces deformation in the surface [26].

The bearing area curves of Al 6061 and NiP_SS316L surfaces are shown in Figures 11 and 12, respectively. The proportion of the reduced valley depth is increased on the aluminum surface after the line polishing experiments. It confirms that though the surface is getting finished, it undergoes deeper abrasive indentation, which translates to abrasive wear of the surface. On the other hand, the reduced valley depth portion is decreased in the nickel-phosphorus plated surface after the line polishing experiment. It suggests that material is being sheared off quickly, and it reduces the level of core roughness and simultaneously reduces the valley depth. Furthermore, the skewness and the kurtosis of the counter surface play an important role in establishing contact between the surface and the flexible tool. The skewness (Ssk) is defined as the asymmetries of the surface height distributions from the mean plane. If the surface has a symmetrical distribution of peaks and valleys, it has zero skewness. If the surface has an uneven peak height and valley depth distribution, it is called a positive or negative skewed surface, respectively. The higher positive skewness is associated with a higher initial wear rate, whereas higher negative skewness is responsible for better fluid retention capacity.

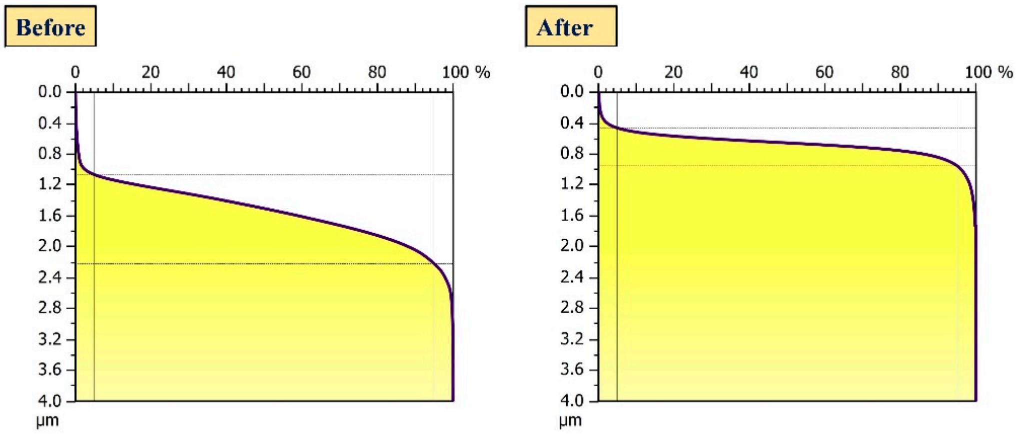

Figure 11. Bearing area curve (BAC) of Al 6061 surface.

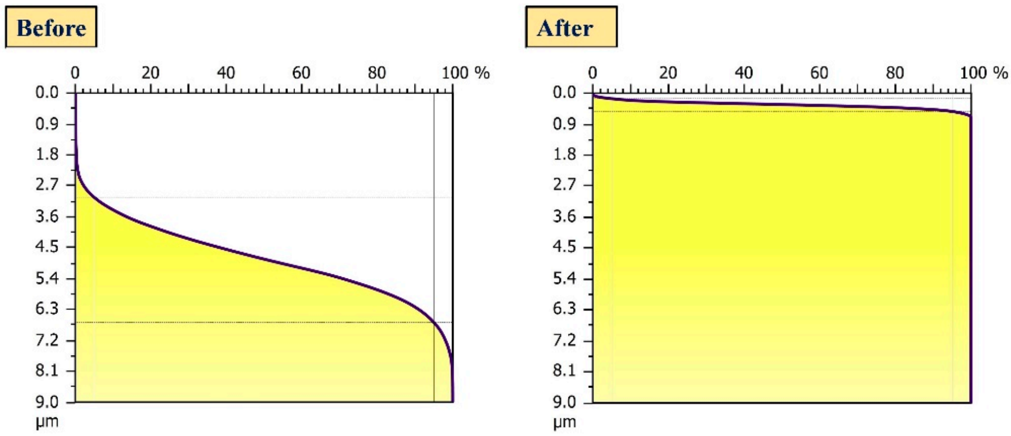

Figure 12. Bearing area curve (BAC) of NiP_SS316L surface.

The sharpness of the asperities on the surface can be examined by kurtosis (Sku). The Gaussian surface has a kurtosis value of 3. The surface with a kurtosis value greater than 3 has centrally distributed irregularities, whereas the equally distributed surface has a kurtosis value less than 3. The skewness and kurtosis values are studied to understand more about the distribution of the asperities and the sharpness of the peaks, as given in Table 4. The higher kurtosis for the Al 6061 surface can be associated with abrasion by abrasive particles.

Table 4. Surface texture parameters for tribology and bearing area curve (BAC).

	Skewness (Ssk)	**Kurtosis (Sku)**
Al 6061 (Before)	−0.541	3.773
Al 6061 (After)	−1.673	10.938
NiP_SS316L (Before)	−0.060	3.328
NiP_SS316L (After)	−0.304	3.024

3.4. Characterization of the Used Tools

The wear mechanisms of the tool surface can be studied through SEM micrographs. Figures 13 and 14 show the SEM images of the flexible abrasive tool used for line polishing Al 6061 and NiP_SS316L surfaces, respectively. The primary wear mechanisms observed in the tool used for the aluminum surface are adhesion, roll formation, and fatigue. It can be observed that the materials, along with abrasive particles, are being pulled out, resulting in the adhesive wear of the tool [11]. The small ridges found around the tool surface are actually roll formations of the pulled material. In some places, it is observed that a linear void is created that can be termed fatigue of the outer surface of the tool. The intensity of the interaction between the abrasives and the soft tool will initiate surface degradation and material deformation [27]. As the aluminum surface has difficulty in machining, it can be assumed that the surface and material properties also contribute significantly to the wear of the soft tool.

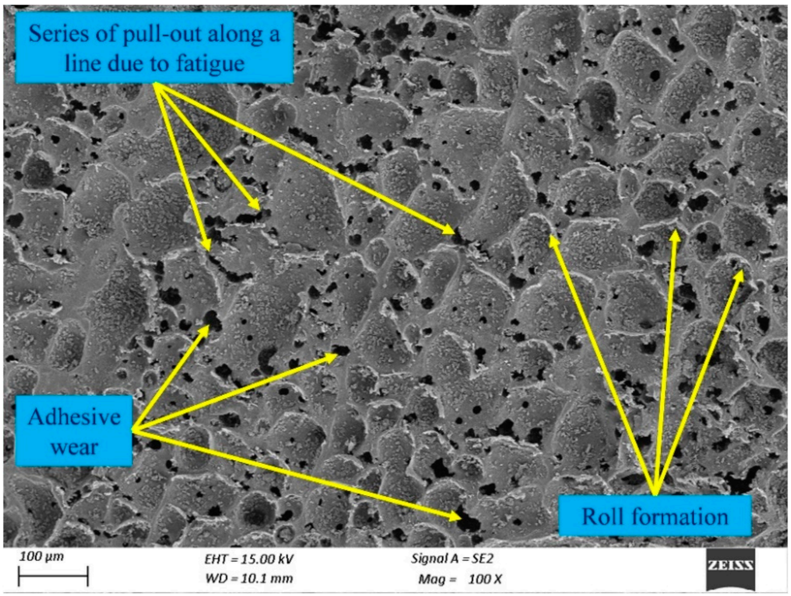

Figure 13. SEM image of used flexible abrasive tool after line polishing on Al 6061.

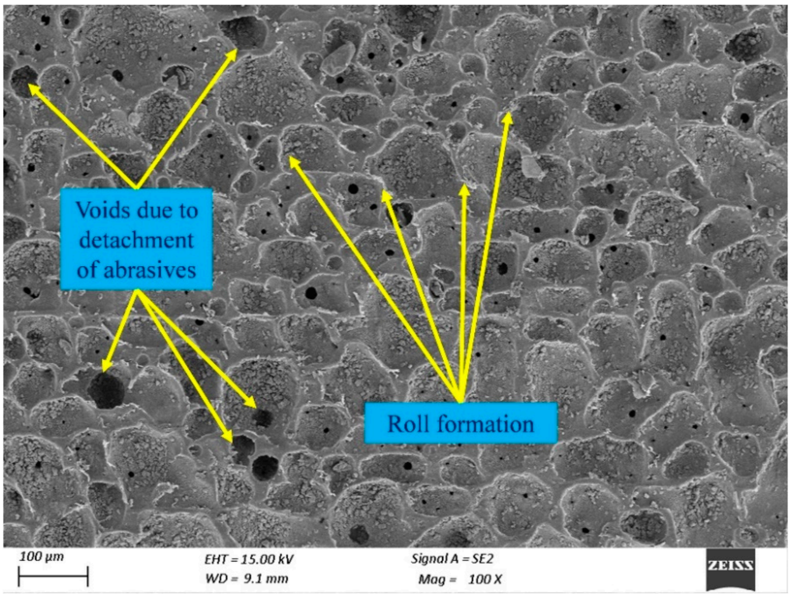

Figure 14. SEM image of used flexible abrasive tool after line polishing on NiP_SS316L.

The primary wear mechanisms observed in the tool used for the nickel-phosphorus-plated surface are abrasion and roll formation. It can be observed that the abrasives are detached from the surfaces, indicating the wear of the surface. Roll formation is common, whereas detached abrasives create voids on the surface. It can be further explained as the cluster of blunt abrasive particles formed after detachment, resulting in abrasion of the soft tool. These detached abrasive particles are mostly blunt, and they do not affect the integrity of the finished surface much. This interaction between the soft tool, the loose abrasives, and the counter surface is called a three-body abrasion.

Elemental mapping of the tool utilized for the Al 6061 surface shown in Figure 15 verifies the presence of aluminum alloy 6061 constituents. It supports the statement that the outer surface of the tool is loaded with chips. Additionally, the presence of abrasive particles shows that the tool is self-replenishing because they are also present on the outer surface and effectively remove the material from the surface.

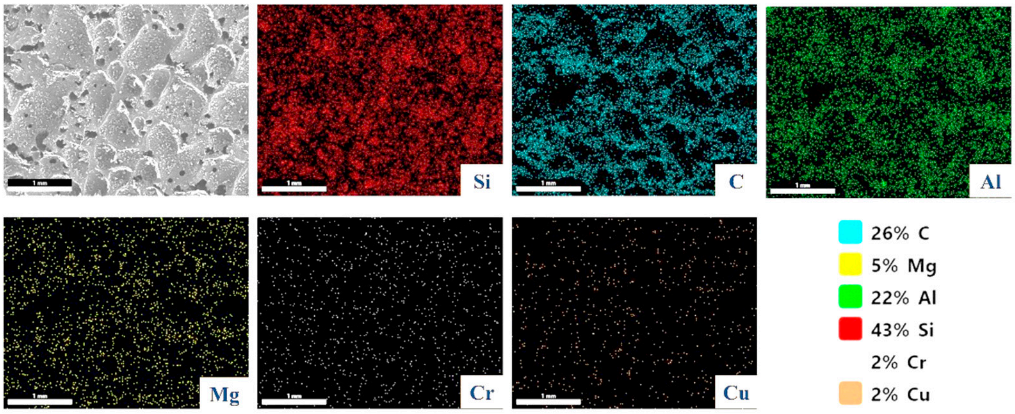

Figure 15. Elemental mapping of used flexible abrasive tool after line polishing on Al 6061.

Similar findings are drawn using the elemental mapping of the tool used for NiP_SS316L shown in Figure 16. Along with the iron and chromium particles, nickel and phosphorus are visible, indicating that the tool is loaded with the base material. The presence of abrasive particles following tool wear and loading is evidence of the self-replenishing capability. EDS can detect both major elements with concentrations higher than 10 wt.% and minor elements with concentrations of 1 wt.% to 10 wt.%. The constituents of workpiece material are observed in the elemental mapping of the used tool. Tools are soaked in DI water before finishing, but these tools are dried before the EDS. As a result, the chance of contamination with other materials other than constituents of workpiece materials is very less. A larger scan area is considered for Figures 15 and 16 as compared to Figure 5 because the used tool is likely to be loaded with chips, and it is difficult to capture abrasives, as well as the chips adhered to the surface precisely in a smaller scan area. The abrasive particles used in this study are of 4 µm size, and the scan area used in elemental mapping is much higher as compared to the abrasive size, so it can correctly capture the presence of abrasive particles.

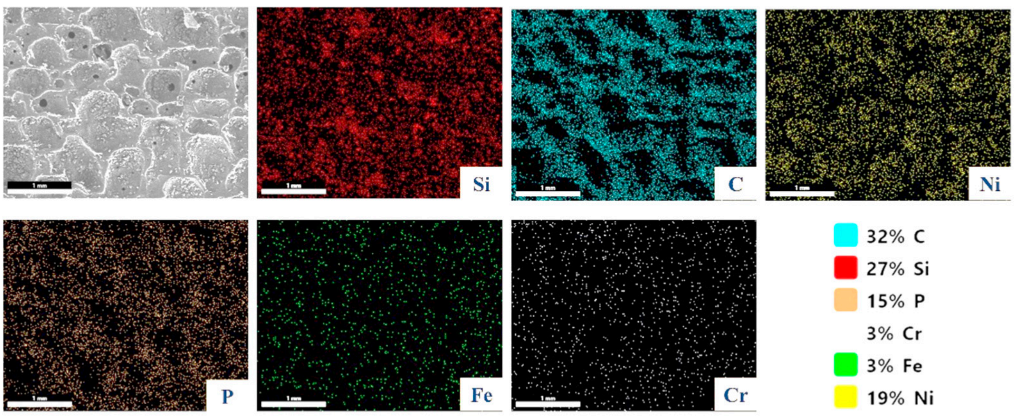

Figure 16. Elemental mapping of used flexible abrasive tool after line polishing on NiP_SS316L.

The initial roughness of the counter surface plays a vital role in tool wear. The tool life is longer when used against a smooth and semi-rough surface. Moreover, the sliding distance has a significant impact on the wear rate [28]. Different numerical simulations and analytical estimations are performed to predict the wear volume of elastomers based on parameters such as contact pressure, sliding velocity, and roughness of the counter surface. However, a still comprehensible prediction of elastomeric wear requires more extensive research on multiscale modeling [19].

$$\text{Wear rate (mg/min)} = \frac{\text{Total weight loss}}{\text{Running time}} \tag{2}$$

The weight loss ratio to the overall finishing time can be used to define the wear rate of the tool, as given in Equation (2). Figure 17 shows the tool weight before and after performing the line polishing. The calculated wear rate for Al 6061 and NiP_SS316L is 10.625 mg/min and 23 mg/min, respectively. A correlation has been established between the initial roughness of the counter surface and the wear rate of the tool. The wear rate of the tool is almost twice when the initial areal roughness (Sa) of the electroless nickel-plated surface is 3.5 times that of the aluminum surface. However, tool wear is also affected by the mechanical and thermal properties of the workpiece. There is a chance that the elastomeric tool may soften as the portion of the heat generated due to friction between the tool and workpiece is transferred to the tool material, which in turn impacts the wear of the tool.

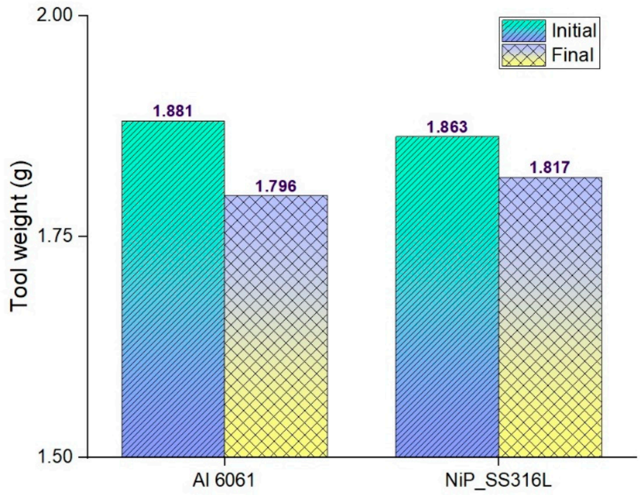

Figure 17. Tool weight before and after performing the finishing experiment.

3.5. Contact Mechanics

The contact between the flexible tool and the workpiece is established by different surface asperities. These asperities support the total normal force acting on the contact interface. Each asperity will carry a fraction of this force. The total contact area A between the workpiece and the flexible tool is given by [29]:

$$A = \frac{F_n}{H} \tag{3}$$

where F_n is the normal force and H is the workpiece hardness (in MPa).

Plastic deformation is predominant on the surface when shear stress exceeds the shear strength.

$$F_t = \tau A \tag{4}$$

where F_t is the tangential force and τ is the shear stress.

The coefficient of friction (CoF), μ, is defined as the force ratio and denoted as:

$$\mu = \frac{F_t}{F_n} = \frac{\tau}{H} \tag{5}$$

The coefficient of friction is not only dependent on tool compression and rotational speed but also on the surface conditions and material properties of the contact. Adhesion and plowing occur when the contact between the tool and workpiece is established through the surface asperities. The minimum force required to shear the contacting asperities is called the adhesion force. When a hard abrasive particle indents into a relatively softer surface, it applies a plowing force. The sum of the plowing and adhesion forces is the total friction force. The transition between elastic and plastic deformation occurs when the shear stress exceeds the critical value. Beyond this point, the material deforms plastically. The tangential force acting at the interface is higher than the interatomic forces in the case of plastic deformation. During the finishing process, the abrasive particles in contact with the workpiece surface are responsible for three phenomena at the contact site. The primary action is the rubbing between the tool and workpiece pair without substantial material removal. It is followed by the plowing action, where the material is plastically deformed. The final action is cutting, where the material is removed due to shearing. The material removal in the flexible abrasive tool finishing depends on the indentation and shearing of the abrasive particles.

There are two stress components acting on the surface. The normal stress component (σ) acts perpendicular to the surface, whereas the shear stress component (τ) acts in the direction parallel to the surface. The stress components are dependent on the contact area.

$$\sigma = \frac{F_{\mathrm{n}}}{A} \tag{6}$$

$$\tau = \frac{F_{\mathrm{t}}}{A} \tag{7}$$

$$\mu = \frac{F_{\mathrm{t}}}{F_{\mathrm{n}}} = \frac{\tau}{\sigma} \tag{8}$$

The tool is subjected to normal compressive stress and shear stress. The failure of a material occurs when shear stress is higher than the material's shear strength. As aluminum is a soft material with a sticking tendency, the CoF is higher, as seen in the experimental data. The stress state of an element and Mohr's circle are shown in Figure 18.

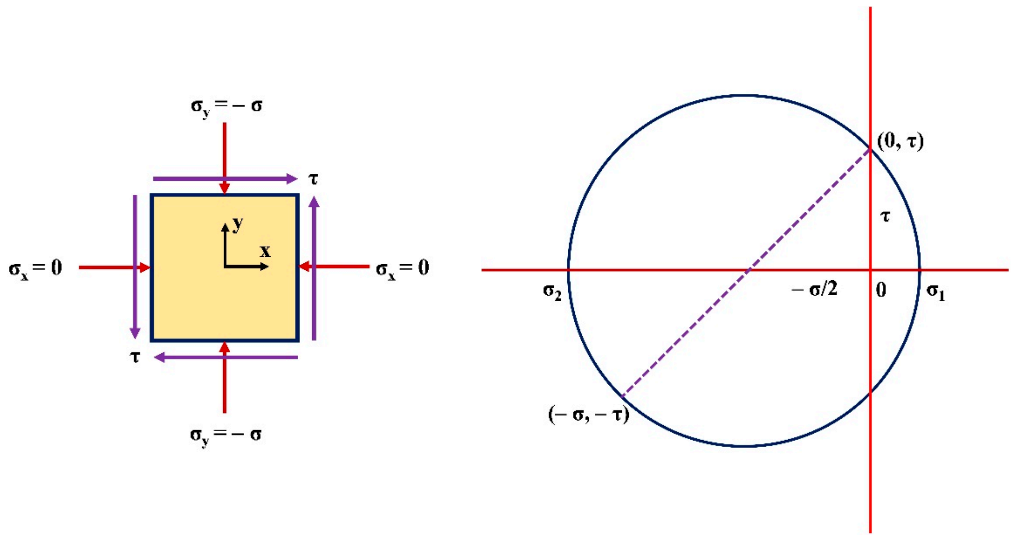

Figure 18. Stress state of an element and the Mohr's circle for the corresponding element on the tool surface.

From Figure 18, Mohr's circle radius is calculated as

$$\text{Radius of the Mohr's circle} = \sqrt{\tau^2 + \left(\frac{|\sigma|}{2}\right)^2} \quad (9)$$

The two principal stresses σ_1 and σ_2 can be obtained using the radius of Mohr's circle as given by Equations (10) and (11).

$$\sigma_1 = -\frac{|\sigma|}{2} + \sqrt{\tau^2 + \left(\frac{|\sigma|}{2}\right)^2} \quad (10)$$

$$\sigma_2 = -\frac{|\sigma|}{2} - \sqrt{\tau^2 + \left(\frac{|\sigma|}{2}\right)^2} \quad (11)$$

Using Equation (8), the principal stresses can be expressed in terms of the coefficient of friction μ. Among the two principal stresses, the tool material is likely to fail due to the positive principal stress (σ_1). Figure 19 shows the ratio of principal stress to normal stress with respect to the coefficient of friction.

$$\sigma_1 = \frac{|\sigma|}{2}\left(\sqrt{4\mu^2 + 1} - 1\right) \quad (12)$$

$$\sigma_2 = -\frac{|\sigma|}{2}\left(\sqrt{4\mu^2 + 1} + 1\right) \quad (13)$$

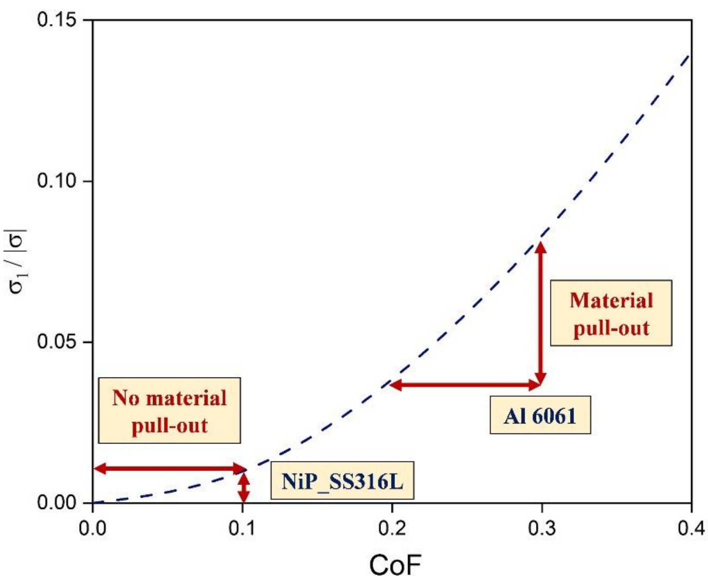

Figure 19. Ratio of principal stress to normal stress with respect to coefficient of friction.

Tool material is likely to have pull-outs with an increase in frictional coefficient. A higher frictional coefficient is likely to alter the tool surface, thus affecting the performance of the tool. It can be concluded that the failure of the material is related to operating conditions and the properties of the counter surface. The hardness of the aluminum alloy is relatively lower than the electroless nickel-plated surface. Moreover, the tool wear can follow a similar trend if the shear stress component is higher than the critical value in the case of a nickel-plated surface.

4. Conclusions

Fabricated flexible abrasive tools are used to study the wear behavior and quality of the finished surfaces in line polishing experiments. From this work, the following conclusions can be made:

1. Elastomeric tools with embedded abrasive particles are fabricated by solvent casting. Fabricated tools have an open-cell porous structure for fluid retention.
2. Wear mechanisms are found to be a combination of adhesion, abrasion, roll formation, and fatigue.
3. The elastic properties of tool material are measured using dynamic mechanical analysis (DMA) and Shore A durometer. The storage modulus obtained in DMA, which represents the elastic properties of the tool, is close to the elastic modulus obtained from Gent's equation using shore A hardness value.
4. The normal cutting forces decrease at the beginning from the peak value, and after that, it stabilizes. It can be attributed to initial tool wear related to abrasion and adhesion.
5. The elemental mapping confirms tool loading at the outer surface. Moreover, the wear rate of an abrasive tool interacting with the rough counter surface is more as compared to the surface having lower roughness.
6. The finishing performance of the tool is also analyzed, and it is observed that a considerable reduction in Sa is obtained after the single pass line polishing experiments. After a single pass of 2 min, the surface roughness of Al 6061 and NiP_SS316L is 112 nm and 84 nm, respectively.
7. The finishing rate is higher in comparison to previous works related to the finishing of these materials. Furthermore, when compared to other finishing processes, such as diamond turning, magnetorheological finishing, and chemo-mechanical polishing, the advantages of flexible abrasive tool finishing include low fabrication costs, uniform finishing, and negligible wastage. The results obtained in this work can be improved by modifying the fabrication technique of flexible tools in such a way that the pore size of the tools can be increased in order to accommodate more chips without affecting the performance of the tools.

Author Contributions: Conceptualization, visualization, M.K., A.S. and V.R.; methodology, validation, formal analysis, investigation, writing—original draft preparation, M.K.; writing—review and editing, M.K., A.S. and V.R.; supervision, resources, project administration, A.S. and V.R. All authors have read and agreed to the published version of the manuscript.

Funding: This research was funded by the Space Applications Centre (SAC) of the Indian Space Research Organization (ISRO).

Data Availability Statement: Not applicable.

Acknowledgments: The authors thank ENP Techno Engineers, Ahmedabad, India, for providing an electroless nickel plating service.

Conflicts of Interest: The authors declare no conflict of interest.

References

1. Hakami, F.; Pramanik, A.; Basak, A.K.; Ridgway, N. Elastomers' wear: Comparison of theory with experiment. *Tribol. Int.* **2019**, *135*, 46–54. [CrossRef]
2. Wu, Y.P.; Zhou, Y.; Li, J.L.; Zhou, H.D.; Chen, J.M.; Zhao, H.C. A comparative study on wear behavior and mechanism of styrene butadiene rubber under dry and wet conditions. *Wear* **2016**, *356*, 1–8. [CrossRef]
3. Lancaster, J.K. Relationships Between the Wear of Polymers and their Mechanical Properties. *Proc. Inst. Mech. Eng. Conf. Proc.* **1968**, *183*, 98–106. [CrossRef]
4. Rhee, S.K. Wear equation for polymers sliding against metal surfaces. *Wear* **1970**, *16*, 431–445. [CrossRef]
5. Viswanath, N.; Bellow, D.G. Development of an equation for the wear of polymers. *Wear* **1995**, *181*, 42–49. [CrossRef]
6. Panda, S.; Chowdhury, S.R.; Sarangi, M. Effects of non-Gaussian counter-surface roughness parameters on wear of engineering polymers. *Wear* **2015**, *332*, 827–835. [CrossRef]
7. Schallamach, A. How does rubber slide? *Wear* **1971**, *17*, 301–312. [CrossRef]

8. Ligier, K.; Olejniczak, K.; Napiórkowski, J. Wear of polyethylene and polyurethane elastomers used for components working in natural abrasive environments. *Polym. Test.* **2021**, *100*, 107247. [CrossRef]
9. Belkhir, N.; Bouzid, D.; Herold, V. Morphological behavior and wear of polyurethane pads used in glass polishing process. *Precis. Eng.* **2012**, *36*, 641–649. [CrossRef]
10. Castillo-Mejia, D.; Gold, S.; Burrows, V.; Beaudoin, S. The effect of interactions between water and polishing pads on chemical mechanical polishing removal rates. *J. Electrochem. Soc.* **2013**, *150*, G76. [CrossRef]
11. Kumar, M.; Sidpara, A.M.; Racherla, V. Surface finishing of aluminium 6061 using fabricated flexible abrasive tool. *Mater. Today Commun.* **2022**, *33*, 104614. [CrossRef]
12. Lloyd, A.I.G.; Noel, R.E.J. The effect of counterface surface roughness on the wear of UHMWPE in water and oil-in-water emulsion. *Tribol. Int.* **1988**, *21*, 83–88. [CrossRef]
13. Amenta, F.; Bolelli, G.; De Lorenzis, S.; Bertarini, A.; Lusvarghi, L. Tribological Behavior of Reinforced PTFE Composites and Un-Reinforced Polyketone-Based Materials against Coated Steel. *Lubricants* **2021**, *10*, 5. [CrossRef]
14. Quaglini, V.; Dubini, P.; Ferroni, D.; Poggi, C. Influence of counterface roughness on friction properties of engineering plastics for bearing applications. *Mater. Des.* **2009**, *30*, 1650–1658. [CrossRef]
15. Nunez, E.E.; Polycarpou, A.A. The effect of surface roughness on the transfer of polymer films under unlubricated testing conditions. *Wear* **2015**, *326*, 74–83. [CrossRef]
16. Wang, C.; Stiller, T.; Hausberger, A.; Pinter, G.; Grün, F.; Schwarz, T. Correlation of Tribological Behavior and Fatigue Properties of Filled and Unfilled TPUs. *Lubricants* **2019**, *7*, 60. [CrossRef]
17. Wang, C.; Hausberger, A.; Berer, M.; Pinter, G.; Grün, F.; Schwarz, T. Fretting Behavior of Thermoplastic Polyurethanes. *Lubricants* **2019**, *7*, 73. [CrossRef]
18. Kumar, M.; Sidpara, A.M.; Racherla, V. Finishing of OFHC copper using fluid filled open-cell porous flexible abrasive impregnated tools. *Proc. Inst. Mech. Eng. Part B J. Eng. Manuf.* **2022**, 09544054221111879. [CrossRef]
19. Harish, A.B.; Wriggers, P. Modeling of two-body abrasive wear of filled elastomers as a contact-induced fracture process. *Tribol. Int.* **2019**, *138*, 16–31. [CrossRef]
20. Yang, A.C.; Ayala, J.E.; Bell, A.; Scott, J.C. Effects of filler particles on abrasive wear of elastomer-based composites. *Wear* **1991**, *146*, 349–366. [CrossRef]
21. Guo, L.; Zhang, X.; Lee, C.H.; Marinescu, I.D.; Zhang, Y.; Hui, J. An experimental study on the abrasive machining process of electronic substrate material with a novel ultraviolet-curable resin bond diamond lapping plate. *IEEE Access* **2019**, *7*, 64375–64385. [CrossRef]
22. Hill, D.J.T.; Killeen, M.I.; O'Donnell, J.H.; Pomery, P.J.; St John, D.; Whittaker, A.K. Laboratory wear testing of polyurethane elastomers. *Wear* **1997**, *208*, 155–160. [CrossRef]
23. Gent, A.N. On the relation between indentation hardness and Young's modulus. *Rubber Chem. Technol.* **1958**, *31*, 896–906. [CrossRef]
24. Ghosh, G.; Kumar, M.; Sidpara, A.M.; Bandyopadhyay, P.P. Tribological aspects of different machining processes. In *Machining and Tribology*, 1st ed.; Pramanik, A., Ed.; Elsevier: Amsterdam, The Netherlands, 2022; pp. 213–238.
25. Kumar, R.; Kumar, S.; Prakash, B.; Sethuramiah, A. Assessment of engine liner wear from bearing area curves. *Wear* **2000**, *239*, 282–286. [CrossRef]
26. Wang, Y.; Mao, J.; Lu, S.; Xu, Z.; Liu, H.; Li, R. A modified approach based on bearing area curve for surface wear characterization. *Ind. Lubr. Tribol.* **2020**, *72*, 273–278. [CrossRef]
27. Rabinowicz, E. *Friction and Wear of Materials*; Wiley and Sons: New York, NY, USA, 1965.
28. Mahesh, V.; Joladarashi, S.; Kulkarni, S.M. Three body abrasive wear assessment of novel jute/natural rubber flexible green composite. *J. Thermoplast. Compos. Mater.* **2021**, *34*, 1566–1576. [CrossRef]
29. Jiménez, A.E.; Bermúdez, M.D. Friction and wear. In *Tribology for Engineers: A Practical Guide*; Davim, J.P., Ed.; Woodhead Publishing: Cambridge, UK, 2011; pp. 33–63.